A generalized equation for the resonance frequencies of a fluid-filled crack

Yuta Maeda and Hiroyuki Kumagai

Graduate School of Environmental Studies, Nagoya University, Nagoya, Japan. E-mail: maeda@seis.nagoya-u.ac.jp

SUMMARY

Although a model of the resonance of a rectangular fluid-filled crack (crack model) is one of the most frequently used source models of long-period seismic events at volcanoes, there has been no analytical solution for the resonance frequencies. We previously proposed an empirical expression for the resonance frequencies as a mathematical function of the crack length, aperture, and properties of the fluid and the surrounding elastic medium. However, the expression contained an empirical constant that had to be investigated numerically for each crack aspect ratio and oscillation mode, a requirement that prevented widespread use of the expression. In the present study, we examined the theoretical basis for the expression. We assumed that the ratio of the crack wall displacement to the fluid pressure near each crack edge varied as the square root of the distance from the edge. Using this assumption, we showed theoretically that the previously proposed empirical analytical expression was a good approximation (difference ≤2 per cent) to another more complete expression. This theoretical expression is a closed form of a mathematical function of the crack model parameters and oscillation mode number; there are no empirical constants to be determined numerically. The expression thus enabled us to analytically compute the resonance frequencies for arbitrary rectangular cracks, and the results were in good agreement (difference ≤5 per cent) with numerical solutions. Resonance frequencies of cracks can be very easily predicted using this expression. This predictive ability may enhance our quantitative understanding of the processes that generate long-period events at volcanoes.

Key words: Interface waves; Volcano seismology; Theoretical seismology.

1 INTRODUCTION

Long-period (LP) seismic events are common phenomena at volcanoes and are considered to be generated by fluid-related processes (e.g. Chouet & Matoza 2013). Several different source models of LP events have been proposed so far, including resonances of spherical (e.g. Kubotera 1974) and cylindrical (e.g. Chouet 1985) fluid-filled containers, nonlinear self-excited oscillations induced by a fluid flow (Julian 1994) and slow-rupture failure in unconsolidated volcanic materials (Bean *et al.* 2014). Among these explanations, the resonance of a fluid-filled crack (Chouet 1986; Kumagai & Chouet 2000) is one of the most commonly used models of the processes that generate LP events. This model has been applied to quantitative interpretations of LP events at, for example, Galeras (Gil Cruz & Chouet 1997), Kusatsu-Shirane (Kumagai *et al.* 2002), Popocatepetl (Arciniega-Ceballos *et al.* 2012), Merapi (Jousset *et al.* 2013) and Papandayan (Syahbana *et al.* 2014) volcanoes. The scenario for this model is a thin rectangular crack filled with an inviscid fluid that is embedded in an infinite elastic medium. The fluid pressure is suddenly perturbed at a certain place in the crack. The result is a resonant oscillation of the crack wall, the

frequency of which depends on the crack geometry, fluid properties and the properties of the surrounding elastic medium.

An advantage of the fluid-filled crack to other models is an ability to explain the observed peak frequencies of volcano-seismic events by moderate-size resonators. For example, the peak frequency of 3.5–7 s for a tremor at Aso volcano, Japan, had been explained by a spherical magma chamber with a diameter of 4–8 km (Kubotera 1974) but was later explained by a crack of a few hundred meters (Chouet 1986). A key feature of a fluid-filled crack model is the interaction between an acoustic wave in the fluid and a crack wall deformation, which generates an interface wave known as a crack wave. In this respect the resonance of a fluid-filled crack is essentially different from acoustic resonances of fluids in a rigid container. In a fluid-filled crack model, the resonance frequencies of higher modes are not integer multiples of the frequency of the fundamental mode because of the dispersive nature of the crack wave. Because of the interaction between the fluid pressure and crack wall deformation, an analytical treatment of the crack model is quite difficult. Indeed, an analytical solution of the resonance is known in the case of an infinite crack (Ferrazzini & Aki 1987), but numerical simulations have been needed to predict the resonance

Table 1. Symbols used in the fluid-filled crack model.

Symbol	Definition	Unit
L	Crack length	m
W	Crack width ($<L$)	m
d	Crack aperture ($\ll W$)	m
ρ_f	Density of the fluid	kg m^{-3}
a	Sound velocity of the fluid	m s^{-1}
ρ_s	Density of the elastic medium	kg m^{-3}
α	P-wave velocity of the elastic medium	m s^{-1}
b	Bulk modulus of the fluid; $\rho_f a^2$	Pa
μ	Rigidity of the elastic medium; $\rho_s \alpha^2/3$	Pa
C	Crack stiffness; $(b/\mu)(L/d)$	—
m	Mode number (≥ 2)	—
f_m^L	Resonance frequency of a longitudinal mode (wavelength: $2L/m$)	Hz
f_m^W	Resonance frequency of a transverse mode (wavelength: $2W/m$)	Hz
ϵ_m^L	A positive constant (eq. 9)	—
ϵ_m^W	A positive constant (eq. 10)	—
$v_x^f(x, y, t)$	Fluid velocity (x component) averaged over the crack aperture	m s^{-1}
$v_y^f(x, y, t)$	Fluid velocity (y component) averaged over the crack aperture	m s^{-1}
$u(x, y, t)$	Normal displacement of the crack wall	m
$P(x, y, t)$	Fluid pressure averaged over the crack aperture	Pa

frequencies of a finite crack. Numerical simulations have been conducted with a finite difference method (FDM; Chouet 1986) or a boundary integral method (Yamamoto & Kawakatsu 2008).

We previously proposed an empirical analytical equation for the resonance frequencies of a finite, fluid-filled crack (Maeda & Kumagai 2013). The equation was in the form of a mathematical function of the crack length, aperture, fluid properties and the properties of the surrounding elastic medium, but it contained an empirical constant that depended on the crack aspect ratio and oscillation mode. The requirement to determine the constant numerically for each crack aspect ratio and oscillation mode has prevented widespread use of the equation for interpretations of LP events at volcanoes.

The purpose of the present study was to investigate an analytical expression for the empirical constant as a function of the crack aspect ratio and oscillation mode. We achieved this by examining the theoretical background of the previously proposed expression. The result enabled analytical computations of the resonance frequencies for arbitrary rectangular cracks.

2 DEFINITION OF THE PROBLEM AND PREVIOUS THEORETICAL STUDIES

We consider a 3-D rectangular crack filled with an inviscid fluid that is embedded in an infinite elastic medium. This system is characterized by the crack geometry (L, W and d), fluid properties (ρ_f and a) and the properties of the surrounding elastic medium (ρ_s and α) (Table 1). We assume a Poisson ratio of 0.25 for the elastic medium. The boundary conditions on the crack wall consisted of the continuities of the normal displacement and stress and zero shear stress. We assume continuity of the velocities in the fluid and the elastic medium along the crack edges. The normal displacement and shear stress are set to zero on the crack plane outside the crack. Symmetric and antisymmetric modes with respect to the crack plane are known as the crack resonance. We consider only the symmetric

modes, because antisymmetric modes do not generate a slow wave (Ferrazzini & Aki 1987).

This problem has been solved numerically by Chouet (1986) using a finite difference scheme. He imposed a sudden pressure disturbance at a certain place in the crack and computed the wave field numerically using the equations of motion and constitutive laws in the fluid and elastic medium that were interconnected through the aforementioned boundary conditions on the crack walls and edges. To reduce the computational cost, he averaged the equations of motion and constitutive laws in the fluid over the crack aperture. The results of the averaging were

$$(1/\rho_f)\partial P(x, y, t)/\partial x + \partial v_x^f(x, y, t)/\partial t = 0, \tag{1}$$

$$(1/\rho_f)\partial P(x, y, t)/\partial y + \partial v_y^f(x, y, t)/\partial t = 0, \tag{2}$$

$$(1/b)\partial P(x, y, t)/\partial t + (2/d)\partial u(x, y, t)/\partial t + \partial v_x^f(x, y, t)/\partial x + \partial v_y^f(x, y, t)/\partial y = 0, \tag{3}$$

where t is time, x and y are coordinates along the crack, and the other symbols are defined in Table 1. His numerical solutions showed resonant oscillations of plane waves propagating along the longer (L) and shorter (W) dimensions of the crack. These oscillations have been called longitudinal and transverse modes, respectively (e.g. Gil Cruz & Chouet 1997; Kumagai & Chouet 2000). Based on the simulation results, Chouet (1986) has pointed out that the resonance frequencies are strongly dependent on a non-dimensional constant known as the crack stiffness, $C = (b/\mu)(L/d) = 3(\rho_f/\rho_s)(a/\alpha)^2(L/d)$. In the limit as $C \to 0$ (i.e. $\mu \to \infty$) the resonant oscillation reduces to an acoustic wave in a rigid container, and in the limit as $C \to \infty$ (i.e. $L \to \infty$) the resonant oscillation reduces to a wave in an infinite crack (Ferrazzini & Aki 1987).

The first attempt to interpret these numerically derived characteristics of the crack resonances by analytical means was made by Kumagai (2009). He combined eqs (1)–(3) to remove the tangential fluid velocities v_x^f and v_y^f. The result was

$$\left(\partial^2/\partial t^2\right)\left[P(x, y, t) + (2b/d)u(x, y, t)\right] = a^2\left(\partial^2/\partial x^2 + \partial^2/\partial y^2\right)P(x, y, t). \tag{4}$$

He assumed the crack wall displacement u to be proportional to the fluid pressure P as follows:

$$u(x, y, t) = (\epsilon L/\mu)P(x, y, t), \tag{5}$$

where ϵ is a constant. Inserting eq. (5) into (4) resulted in a wave equation

$$(1 + 2\epsilon C)\left(\partial^2/\partial t^2\right)P(x, y, t) = a^2\left(\partial^2/\partial x^2 + \partial^2/\partial y^2\right)P(x, y, t). \tag{6}$$

Eq. (6) suggests that the resonance frequencies for the longitudinal and transverse modes are

$$f_m^L = ma\big/\left[2L(1 + 2\epsilon C)^{1/2}\right] \tag{7}$$

and

$$f_m^W = ma\big/\left[2W(1 + 2\epsilon C)^{1/2}\right], \tag{8}$$

respectively (Maeda & Kumagai 2013). Here the mode number m for a longitudinal (transverse) mode is defined such that the wavelength is $2L/m$ ($2W/m$). In the case of an infinite crack, u and P are proportional to each other (Ferrazzini & Aki 1987). For a finite crack, however, the two quantities may not necessarily be

Table 2. Symbols related to the coordinate system of Fig. 1.

Symbol	Definition	Longitudinal mode ($\chi < 1$)	Transverse mode ($\chi > 1$)	Unit
L_x	Crack length along x	L	W	m
L_y	Crack length along y	W	L	m
χ	L_y/L_x	W/L	L/W	—
C_x	Crack stiffness along x; $(b/\mu)(L_x/d)$	C	CW/L	—
f_m	Resonance frequency of a mode (wavelength: $2L_x/m$)	f_m^L	f_m^W	Hz
ϵ_m	A positive constant (eq. 11)	ϵ_m^L	$\epsilon_m^W L/W$	—
ϵ_m^{2D}	The ϵ_m value for a 2-D problem	—	—	—

Table 3. Functions introduced in this study.

Symbol	Definition	Unit
$u_m(x, y, t)$	$u(x, y, t)$ for an oscillation mode (wavelength: $2L_x/m$)	m
$P_m(x, t)$	$P(x, y, t)$ for an oscillation mode (wavelength: $2L_x/m$)	Pa
$g_m(x, y)$	Non-dimensional u_m-to-P_m ratio (eq. 13)	—
$g_m^{2D}(x)$	$g_m(x, y)$ for a 2-D problem	—
$\bar{g}_m(x)$	$g_m(x, y)$ averaged over y	—
$a_m(x)$	Local speed of the crack wave (eq. 17)	m s^{-1}
$h_m(\xi)$	Eq. (23)	—
$H_m(\eta)$	Eq. (34)	—
$J_m(\xi)$	Eq. (27)	—
$K_m(\xi)$	Eq. (27)	—

Table 4. Constants introduced in this study.

Symbol	Definition	Unit
λ_m	Wavelength of the crack wall displacement; $2L_x/m$	m
λ_m^P	Wavelength of the fluid pressure; $2L_x/(m-1)$	m
T_m	Roundtrip traveltime of the crack wave	s
N_m	The number of oscillations during roundtrip travel	—
I_m	Eq. (21)	—
γ	Spatial extent of the crack edge effect defined by eq. (23)	—
g_{m0}	The maximum value of $g_m(x, y)$	—
g_{m0}'	Eq. (33)	—
$\hat{g}_m$	Average of $g_m(x, y)$	—
g_{m0}^L	g_{m0}'	—
g_{m0}^W	$g_{m0}' W/L$	—

Figure 1. The coordinate systems for (a) a longitudinal wave and (b) a transverse wave.

proportional to each other, and thus eqs (7) and (8) needed to be evaluated.

This evaluation was made by Maeda & Kumagai (2013), who showed that the resonance frequencies computed numerically were different from those expected from eqs (7) and (8). Then, after some trial and error, they found empirically that the resonance frequencies were well predicted by

$$f_m^L = (m - 1)a \Big/ \left[2L \left(1 + 2\epsilon_m^L C \right)^{1/2} \right] \tag{9}$$

for a longitudinal mode and

$$f_m^W = (m - 1)a \Big/ \left[2W \left(1 + 2\epsilon_m^W C \right)^{1/2} \right] \tag{10}$$

for a transverse mode (the symbols are defined in Table 1). The constants ϵ_m^L and ϵ_m^W are independent of the crack stiffness (C) but dependent on the crack aspect ratio (W/L) and mode number (m). In Maeda & Kumagai (2013), these constants are given to only a few numbers of W/L and m. The equations can therefore not be widely applied to interpretations of LP events at volcanoes.

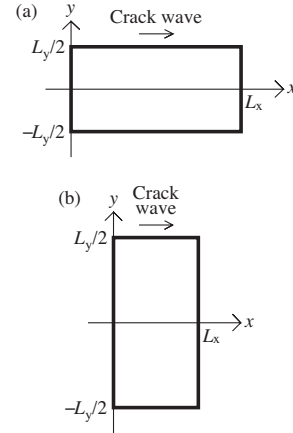# 3 THEORETICAL INVESTIGATION OF THE RESONANCE FREQUENCIES

In this section, we examine the theoretical background for the empirical relationships expressed by eqs (9) and (10), and we derive analytical expressions for ϵ_m^L and ϵ_m^W. Symbols used below are summarized in Tables 2–4.

3.1 The coordinate system

To conveniently develop the theory, we assumed the x and y axes to be parallel and perpendicular, respectively, to the direction of wave propagation direction, and we assumed the crack to lie within the range $0 \leq x \leq L_x$ and $-L_y/2 \leq y \leq L_y/2$, where L_x and L_y

are positive constants (Fig. 1). For a longitudinal wave, $L_x = L$ and $L_y = W$, whereas for a transverse wave, $L_x = W$ and $L_y = L$ (Table 2). We simulated a 2-D crack by taking the limit as $L_y \to \infty$. We used $C_x = (b/\mu)(L_x/d)$ as the crack stiffness along the x direction. Using these symbols, eqs (9) and (10) were rewritten as

$$f_m = (m - 1)a \Big/ \left[2L_x \left(1 + 2\epsilon_m C_x \right)^{1/2} \right]. \tag{11}$$

The constant ϵ_m is independent of C_x but dependent on the crack aspect ratio $\chi = L_y/L_x$ and mode number m.

3.2 Basic equations

For each oscillation mode of wavelength $\lambda_m = 2L_x/m$, eq. (4) gives

$$(\partial^2/\partial t^2)[P_m(x, t) + (2b/d)u_m(x, y, t)] = a^2 \partial^2 P_m(x, t)/\partial x^2. \tag{12}$$

The pressure P_m in eq. (12) is assumed to be independent of y because the crack wave propagates along the x direction, whereas the displacement u_m must depend on y because otherwise the zero displacement boundary conditions on the crack edges cannot be satisfied. We assume that the temporal dependences of u_m and P_m at each location are identical. Based on this assumption, eq. (5) was modified as follows:

$$u_m(x, y, t) = (L_x/\mu)g_m(x, y)P_m(x, t), \tag{13}$$

where g_m is a function of location that does not change with time. Inserting eq. (13) into (12) gives

$$[1 + 2C_x g_m(x, y)]\partial^2 P_m(x, t)/\partial t^2 = a^2 \partial^2 P_m(x, t)/\partial x^2, \tag{14}$$

and averaging this equation over y results in

$$[1 + 2C_x \bar{g}_m(x)]\partial^2 P_m(x, t)/\partial t^2 = a^2 \partial^2 P_m(x, t)/\partial x^2, \tag{15}$$

$$\bar{g}_m(x) = (1/L_y)\int_{-L_y/2}^{L_y/2} g_m(x,y)\mathrm{d}y = (2/L_y)\int_0^{L_y/2} g_m(x,y)\mathrm{d}y, \tag{16}$$

where g_m has been assumed to be symmetric with respect to $y = 0$.

Eq. (15) indicates that P_m propagates at a location-dependent wave velocity

$$a_m(x) = a/[1 + 2C_x\bar{g}_m(x)]^{1/2}. \tag{17}$$

The traveltime of this wave, as it propagates from $x = 0$ to $x = L_x$ and then back to $x = 0$, was calculated as follows:

$$T_m = 2\int_0^{L_x}[1/a_m(x)]\mathrm{d}x = 4\int_0^{L_x/2}[1/a_m(x)]\mathrm{d}x, \tag{18}$$

where g_m was assumed to be symmetric with respect to $x = L_x/2$. The number of oscillations included in this roundtrip travel is given by

$$N_m = 2L_x/\lambda_m^P = m - 1 \tag{19}$$

because the wavelength of P_m is $\lambda_m^P = 2L_x/(m-1)$ for a mode of oscillation for which the wavelength of u_m is $\lambda_m = 2L_x/m$ (Maeda & Kumagai 2013). The resonance frequency of this oscillation mode was then calculated as follows:

$$f_m = N_m/T_m = (m-1)a/(2L_x I_m), \tag{20}$$

where

$$I_m = (2/L_x)\int_0^{L_x/2}[1 + 2C_x\bar{g}_m(x)]^{1/2}\mathrm{d}x. \tag{21}$$

Given a specific form of g_m, we could calculate $\bar{g}_m$ using eq. (16), then I_m from eq. (21) and finally f_m using eq. (20). In this way, the resonance frequencies f_m for arbitrary crack aspect ratios and oscillation modes could be calculated.

3.3 2-D problem

In the case of a 2-D crack, there is no dependence on y, and thus g_m depends on x alone. We assumed the following trial form:

$$g_m^{2D}(x) = g_m^{2D}(L_x - x) = g_{m0}h_m(x) \quad (x < L_x/2), \tag{22}$$

where

$$h_m(\xi) = \begin{cases} (\xi/\gamma\lambda_m)^{1/2} & (\xi < \gamma\lambda_m) \\ 1 & (\xi > \gamma\lambda_m) \end{cases}. \tag{23}$$

Eq. (23) argues that the u_m/P_m ratio near each crack edge is proportional to the square root of the distance from the edge; this assumption is based on an analogy to classical static semi-infinite crack theory (e.g. Sun & Jin 2012). The effect of each crack edge spreads out over a distance $\gamma\lambda_m$ (eq. 23), and we assumed $\gamma < 1/2$, implying that the crack edge does not affect u_m beyond a half wavelength.

Inserting eq. (22) into (21) results in

$$I_m = (2/L_x)\int_0^{L_x/2}[1 + 2g_{m0}C_x h_m(x)]^{1/2}\mathrm{d}x, \tag{24}$$

and because $\gamma\lambda_m < L_x/2$, we have

$$I_m = (2/L_x)\left\{\int_0^{\gamma\lambda_m}[1 + 2g_{m0}C_x(x/\gamma\lambda_m)^{1/2}]^{1/2}\mathrm{d}x \right.$$
$$\left. + \int_{\gamma\lambda_m}^{L_x/2}[1 + 2g_{m0}C_x]^{1/2}\mathrm{d}x\right\}. \tag{25}$$
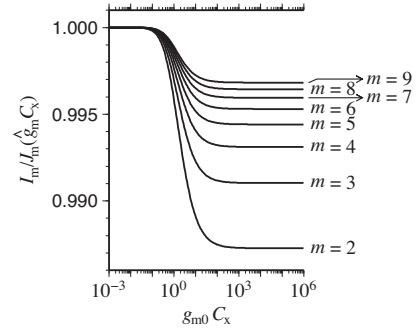

Figure 2. A plot of $I_m/J_m(\hat{g}_m C_x)$ versus $g_{m0}C_x$ for the case $\gamma = 0.22$ calculated using eqs (26), (27) and (29).

The first integral can be calculated by changing the independent variable to $X = (x/\gamma\lambda_m)^{1/2}$, $\mathrm{d}x = 2\gamma\lambda_m X\mathrm{d}X$. The result is

$$I_m = (1 - 4\gamma/5m)J_m(g_{m0}C_x) + (16\gamma/15m)$$
$$\times [1/K_m(g_{m0}C_x) + 1/K_m(g_{m0}C_x)^2], \tag{26}$$

where

$$J_m(\xi) = (1 + 2\xi)^{1/2}, \quad K_m(\xi) = J_m(\xi) + 1. \tag{27}$$

In the derivation of eq. (26), we used the relations $\gamma\lambda_m/L_x = (\gamma/L_x)(2L_x/m) = 2\gamma/m$ and $g_{m0}C_x = [J_m(g_{m0}C_x) + 1][J_m(g_{m0}C_x) - 1]/2$.

The constant g_{m0} represents the maximum amplitude of the function g_m^{2D} (eq. 22). Another useful metric may be the average of g_m^{2D} over x:

$$\hat{g}_m = (1/L_x)\int_0^{L_x} g_m^{2D}(x)\mathrm{d}x = (2/L_x)\int_0^{L_x/2} g_m^{2D}(x)\mathrm{d}x. \tag{28}$$

Inserting eqs (22) and (23) into (28), we obtain a simple relation between g_{m0} and $\hat{g}_m$:

$$\hat{g}_m = (2g_{m0}/L_x)\left[\int_0^{\gamma\lambda_m}(x/\gamma\lambda_m)^{1/2}\mathrm{d}x + \int_{\gamma\lambda_m}^{L_x/2}\mathrm{d}x\right]$$
$$= (1 - 4\gamma/3m)g_{m0}. \tag{29}$$

The value of I_m in eq. (26) is well approximated by $J_m(\hat{g}_m C_x)$. As an example, we show the ratio $I_m/J_m(\hat{g}_m C_x)$ for the case $\gamma = 0.22$ (Fig. 2). The ratio is a decreasing function of C_x, from 1 at $C_x = 0$ to $(1 - 4\gamma/5m)/(1 - 4\gamma/3m)^{1/2}$ at $C_x = \infty$, and this asymptotic value at $C_x = \infty$ is larger than $(1 - 1/5)/(1 - 1/3)^{1/2} \approx 0.98$ because $0 < \gamma < 1/2$ and $m > 2$. This means that $I_m/J_m(\hat{g}_m C_x)$ is between 0.98 and 1 for all possible combinations of C_x, γ and m values, and thus I_m is approximated by $J_m(\hat{g}_m C_x)$ within an error of 2 per cent. With this approximation, eq. (20) reduces to

$$f_m \approx (m-1)a/[2L_x J_m(\hat{g}_m C_x)]$$
$$= (m-1)a/[2L_x(1 + 2\hat{g}_m C_x)^{1/2}]. \tag{30}$$

A comparison of eqs (11) and (30) leads to the interpretation that $\epsilon_m = \hat{g}_m$.

3.4 3-D problem

We assume that the crack edges in the y direction suppressed u_m in the same manner as those in the x direction. Then g_m is given as

$$g_m(x,y) = g_m^{2D}(x)h_m(L_y/2 - |y|). \tag{31}$$

Inserting eqs (31) and (23) into eq. (16) results in

$$\bar{g}_m(x) = (2/L_y)g_m^{2D}(x)\int_0^{L_y/2} h_m(L_y/2 - y)dy = g'_{m0}h_m(x), \quad (32)$$

$$g'_{m0} = g_{m0}H_m(4\gamma/m\chi), \quad (33)$$

where

$$H_m(\eta) = \begin{cases} 1 - \eta/3 & (\eta < 1) \\ 2\eta^{-1/2}/3 & (\eta > 1) \end{cases}. \quad (34)$$

We here used the relation $\lambda_m/L_y = 2L_x/mL_y = 2/m\chi$. The form of $\bar{g}_m$ for the 3-D crack (eq. 32) was the same as that for the 2-D crack (eq. 22), except for the difference between the constants g_{m0} and g'_{m0}. Therefore the 3-D solution was obtained by replacing g_{m0} in the 2-D solution with g'_{m0}, giving

$$I_m = (1 - 4\gamma/5m)J_m(g'_{m0}C_x) + (16\gamma/15m)$$
$$\times [1/K_m(g'_{m0}C_x) + 1/K_m(g'_{m0}C_x)^2]. \quad (35)$$

As was the case in the 2-D problem, this I_m value was approximated by $J_m(\hat{g}_m C_x)$, and the interpretation that $\epsilon_m = \hat{g}_m$ holds, where

$$\hat{g}_m = (1/L_x L_y)\int_0^{L_x} dx \int_{-L_y/2}^{L_y/2} dy g_m(x, y)$$

$$= (2/L_x)\int_0^{L_x/2} dx \bar{g}_m(x)$$

$$= (1 - 4\gamma/3m)g'_{m0}. \quad (36)$$

4 COMPARISONS WITH NUMERICAL SOLUTIONS

The previous section led to the conclusion that $\epsilon_m = \hat{g}_m$ and that the values of $\hat{g}_m$ for 2-D and 3-D cracks are given by eqs (29) and (36), respectively. These conclusions imply the following relationship:

$$\epsilon_m/\epsilon_m^{2D} = g'_{m0}/g_{m0} = H_m(4\gamma/m\chi). \quad (37)$$

To evaluate eq. (37), we estimated the ϵ_m values for various values of χ and m using the FDM code of Chouet (1986). We used fixed values of $L_x/d = 10\,000$, $\rho_f/\rho_s = 1/120$ and $\alpha/a = 5$, which are typical values of LP events at Taal volcano, Philippines (Maeda *et al.* 2013) and correspond to $C_x = 10$. We repeated the FDM computations for χ values from 0.025 to 2 in steps of 0.025. To carry out these calculations, we used 80 fixed grids in L_x and varied the number of grid nodes in L_y from 2 to 160 in steps of 2. Fig. 3(a) shows the resonance frequencies computed by the FDM. The small amplitudes of some of the spectral peaks caused several defects of the resonance frequencies. From the resonance frequencies, we estimated ϵ_m (Fig. 3b) using the relation

$$\epsilon_m = \{[(m-1)a/(2L_x f_m)]^2 - 1\}/(2C_x), \quad (38)$$

which is the inverse of eq. (11). Abrupt changes in the ϵ_m values were caused by the limited resolution of the resonance frequencies; because ϵ_m is a linear function of $1/f_m^2$ (eq. 38), a small change in f_m is significantly amplified by the conversion to ϵ_m when f_m is small. In Fig. 4, we have plotted $\epsilon_m/\epsilon_m^{2D}$ ratios against $1/(m\chi)$, where the ϵ_m^{2D} values were also estimated by the FDM for $C_x = 10$. The relation between $1/(m\chi)$ and $\epsilon_m/\epsilon_m^{2D}$ was independent of the oscillation mode m.
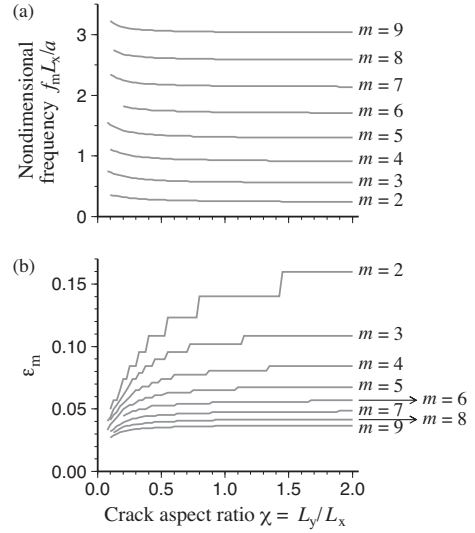

Figure 3. (a) Resonance frequencies f_m for various crack aspect ratios computed with the FDM code, and (b) corresponding ϵ_m values calculated with eq. (38).
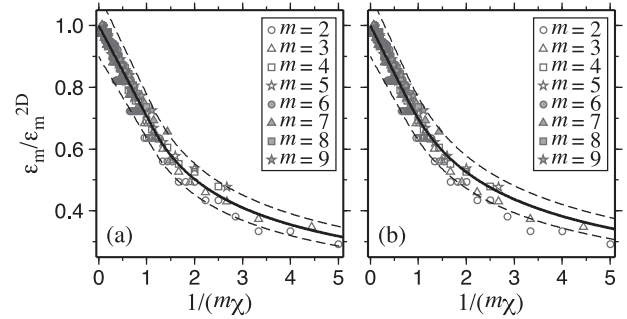

Figure 4. The $\epsilon_m/\epsilon_m^{2D}$ ratios estimated with the FDM and plotted against $1/(m\chi)$ (symbols). The bold lines represent (a) eq. (37) with $\gamma = 0.22$ and (b) eq. (42) with $\gamma = 0.36$. The dashed lines are $1.1\epsilon_m/\epsilon_m^{2D}$ and $0.9\epsilon_m/\epsilon_m^{2D}$ based on these equations.

To compare the data in Fig. 4 with eq. (37), we conducted a grid search for γ from 0.01 to 0.49 in increments of 0.01. For each γ, we calculated the misfit

$$E = \left[\sum_i (d_i^{num} - d_i^{ana})^2 / \sum_i (d_i^{num})^2 \right]^{1/2}, \quad (39)$$

where d_i^{num} is the ith datum of $\epsilon_m/\epsilon_m^{2D}$ obtained with the FDM and d_i^{ana} is the value of $\epsilon_m/\epsilon_m^{2D}$ for the corresponding $1/(m\chi)$ calculated with eq. (37). The minimum E value of 2.29 per cent was obtained with $\gamma = 0.22$ (Fig. 5). Using this γ, the $\epsilon_m/\epsilon_m^{2D}$ ratios were described well by eq. (37) (Fig. 4a). In Fig. 4(a), we have also plotted
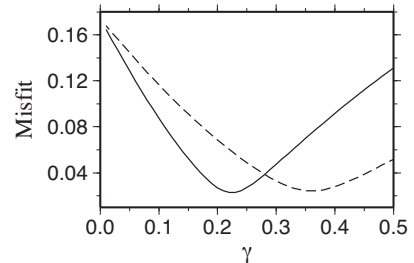

Figure 5. The misfits E (eq. 39) between the $\epsilon_m/\epsilon_m^{2D}$ ratios estimated with the FDM and calculated with eqs (37) (solid line) and (42) (dashed line).

$1.1\epsilon_m/\epsilon_m^{2D}$ and $0.9\epsilon_m/\epsilon_m^{2D}$ to show differences of ± 10 per cent from the equation. Most of the numerically estimated $\epsilon_m/\epsilon_m^{2D}$ ratios were within this range, indicating that eq. (37) with $\gamma = 0.22$ can predict $\epsilon_m/\epsilon_m^{2D}$ to within an error of 10 per cent. The error propagation law and eq. (11) suggest that

$$(\sigma_{fm}/f_m)^2 = (\partial f_m/\partial\epsilon_m)^2(\epsilon_m/f_m)^2(\sigma_{\epsilon m}/\epsilon_m)^2$$
$$= [(\epsilon_m C_x)/(1 + 2\epsilon_m C_x)]^2(\sigma_{\epsilon m}/\epsilon_m)^2, \tag{40}$$

where σ_{fm} and $\sigma_{\epsilon m}$ represent the standard deviations of f_m and ϵ_m, respectively. Because $(\epsilon_m C_x)/(1 + 2\epsilon_m C_x)$ is less than $1/2$, we can expect that a 10 per cent error in ϵ_m would be mapped to an error in f_m of at most 5 per cent; if the equation is used with a given m and C_x to investigate the crack length from the observed peak frequencies of an LP event, the result would differ by less than 5 per cent from a numerical estimate.

Until now, we assumed that the u_m/P_m ratio near each crack edge varied as the square root of the distance from the edge (eq. 23). This assumption was based on an analogy to static, semi-infinite crack theory. Another candidate for the u_m/P_m ratio may be an ellipsoidal shape

$$h'_m(\xi) = \begin{cases} \{1 - [(\gamma\lambda_m - \xi)/(\gamma\lambda_m)]^2\}^{1/2} & (\xi < \gamma\lambda_m) \\ 1 & (\xi > \gamma\lambda_m) \end{cases}, \tag{41}$$

which is an analogy to static finite crack theory (e.g. Sun & Jin 2012). In this case, instead of eqs (34) and (37), we have

$$\epsilon_m/\epsilon_m^{2D} = H'_m(4\gamma/m\chi), \tag{42}$$

$$H'_m(\eta) = \begin{cases} 1 - (1 - \pi/4)\eta & (\eta < 1) \\ \pi\eta/4 - (\eta/2)\arcsin(1 - 1/\eta) & (\eta > 1) \\ \quad -[(\eta - 1)/2][1 - (1 - 1/\eta)^2]^{1/2} \end{cases}. \tag{43}$$

Using eq. (42) instead of (37), we obtained a minimum E value of 2.43 per cent with $\gamma = 0.36$ (Fig. 5); this E value was slightly larger than the value of 2.29 per cent from eq. (37). Although the difference in E values between the two cases was small, eq. (42) systematically overestimated the $\epsilon_m/\epsilon_m^{2D}$ ratios for $1/(m\chi) \geq 2$ (Fig. 4b), suggesting that eq. (37), which was derived from the square root model of the u_m/P_m ratio, was a better approximation.

5 MODE NUMBER DEPENDENCE OF ϵ_m FOR A 2-D CRACK

We obtained an analytical expression for $\epsilon_m/\epsilon_m^{2D}$ in the previous section (eq. 37), and the remaining task is an analytical expression for ϵ_m^{2D}. In Maeda & Kumagai (2013), the ϵ_m^{2D} values for $m \leq 9$ were estimated from the resonance frequencies computed by the FDM. For higher oscillation modes, stable estimates of the resonance frequencies are difficult because the number of grid nodes in a wavelength is small. However, we found the ϵ_m^{2D} values for $m \leq 9$ to be inversely proportional to m (Fig. 6), and by extrapolating this relationship, we were able to estimate ϵ_m^{2D} for larger m. The best-fit such relationships were $\epsilon_m^{2D} = 0.3376/m$ for the ϵ_m^{2D} values estimated by varying L_x/d, $\epsilon_m^{2D} = 0.3380/m$ for those estimated by varying ρ_f/ρ_s, and $\epsilon_m^{2D} = 0.3494/m$ for those estimated by varying α/a. Fitting the ϵ_m^{2D} values for all three cases yielded $\epsilon_m^{2D} = 0.3417/m$. The proportionality constants were around 0.34 in all cases, and taking into account the relation $\epsilon_m^{2D} = g_{m0}(3m - 4\gamma)/(3m)$ (eq. 29), we could naturally interpret these fitting lines as

$$\epsilon_m^{2D} = 1/(3m), \tag{44}$$
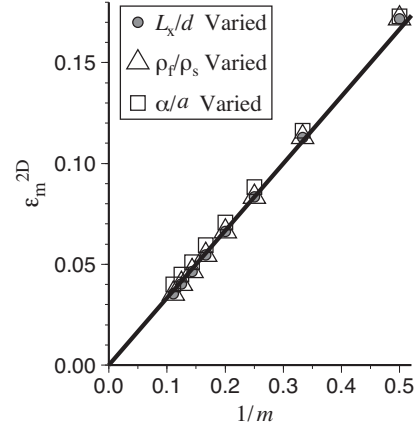
$$g_{m0} = 1/(3m - 4\gamma). \tag{45}$$

Figure 6. The ϵ_m values for a 2-D crack (ϵ_m^{2D}) plotted against $1/m$. Shown are the data in table 1 of Maeda & Kumagai (2013). Circles, triangles and squares indicate the ϵ_m values estimated by varying L_x/d, ρ_f/ρ_s and α/a, respectively. The solid black line corresponds to eq. (44).

6 EXPLICIT EQUATIONS FOR THE RESONANCE FREQUENCIES

We investigated theoretical expressions for the resonance frequencies (eqs 20 and 35). The g'_{m0} value in eq. (35) was calculated with eqs (33) and (45), or explicitly

$$g'_{m0} = \begin{cases} (1 - 4\gamma/3m\chi)/(3m - 4\gamma) & (\chi > 4\gamma/m) \\ (2/3)(m\chi/4\gamma)^{1/2}/(3m - 4\gamma) & (\chi < 4\gamma/m) \end{cases}. \tag{46}$$

Because $\gamma = 0.22$, $4\gamma/m$ is smaller than 1 regardless of m. Therefore, the equation for $\chi > 4\gamma/m$ always applies to the transverse mode ($\chi > 1$). Then, using Table 2, we obtained

$$f_m^L = (m - 1)a/\left(2L I_m^L\right), \tag{47}$$

$$I_m^L = (1 - 4\gamma/5m)J_m\left(g_{m0}^L C\right) + (16\gamma/15m)$$
$$\times \left[1/K_m\left(g_{m0}^L C\right) + 1/K_m\left(g_{m0}^L C\right)^2\right], \tag{48}$$

and

$$g_{m0}^L = \begin{cases} (2/3)(mW/4\gamma L)^{1/2}/(3m - 4\gamma) & (W/L < 4\gamma/m) \\ (1 - 4\gamma L/3mW)/(3m - 4\gamma) & (4\gamma/m < W/L < 1) \end{cases} \tag{49}$$

for a longitudinal mode and

$$f_m^W = (m - 1)a/\left(2W I_m^W\right), \tag{50}$$

$$I_m^W = (1 - 4\gamma/5m)J_m\left(g_{m0}^W C\right) + (16\gamma/15m)$$
$$\times \left[1/K_m\left(g_{m0}^W C\right) + 1/K_m\left(g_{m0}^W C\right)^2\right], \tag{51}$$

and

$$g_{m0}^W = (W/L)(1 - 4\gamma W/3mL)/(3m - 4\gamma) \tag{52}$$

for a transverse mode. Eqs (47)–(52) can be used to compute the resonance frequencies for arbitrary W/L and m.

For practical purposes, the resonance frequencies can be approximated by a simpler version of eq. (11) with errors of less than 2 per cent (Fig. 2). The ϵ_m value of this equation is calculated from eqs (37) and (44) as

$$\epsilon_m = \begin{cases} (1/3m)(1 - 4\gamma/3m\chi) & (\chi > 4\gamma/m) \\ (2/9m)(m\chi/4\gamma)^{1/2} & (\chi < 4\gamma/m) \end{cases}. \tag{53}$$
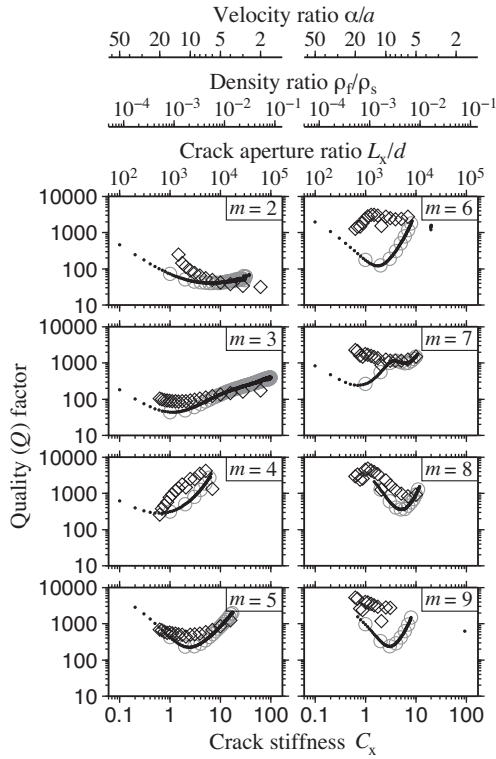
Figure 7. The quality (Q) factors of 2-D cracks corrected for numerical damping. Dots, circles and diamonds represent the results obtained by varying L_x/d, ρ_f/ρ_s and α/a, respectively.

The resonance frequency of a longitudinal mode is then calculated with eq. (9) and

$$\epsilon_m^L = \begin{cases} (2/9m)(mW/4\gamma L)^{1/2} & (W/L < 4\gamma/m) \\ (1/3m)(1 - 4\gamma L/3mW) & (4\gamma/m < W/L < 1) \end{cases},\quad (54)$$

and that of a transverse mode is calculated with eq. (10) and

$$\epsilon_m^W = (W/L)(1/3m)(1 - 4\gamma W/3mL),\quad (55)$$

where $\gamma = 0.22$.

7 THE QUALITY (Q) FACTORS

In addition to the peak frequencies, the quality (Q) factors of observed waveforms of LP events have been used to estimate the geometry and fluid properties of the source crack (e.g. Kumagai *et al.* 2002). No analytical expression for the Q factors has been proposed. We tried to estimate an expression for Q empirically using the FDM code of Chouet (1986). We focused on a 2-D problem and conducted the following three sets of FDM computations: (1) varying L_x/d from 100 to 100 000 in increments of 100 with fixed values of $\rho_f/\rho_s = 1/120$ and $\alpha/a = 5$; (2) varying ρ_f/ρ_s from 1/1200 to 1/12 in increments of 1/1200 with fixed values of $L_x/d = 10\,000$ and $\alpha/a = 5$; and (3) varying α/a from 2 to 20 in increments of 1 with fixed values of $L_x/d = 10\,000$ and $\rho_f/\rho_s = 1/120$. Fig. 7 shows the Q factors estimated by the FDM using the approach described in Appendix A. The Q factors estimated by varying α/a showed a different pattern from the other two cases, but those estimated by varying L_x/d and ρ_f/ρ_s were almost identical to each other (Fig. 7), suggesting that the Q factors do not depend on L_x/d and ρ_f/ρ_s separately but depend on these parameters only through C_x. We note that the resonance frequency f_m also depends on L_x/d and ρ_f/ρ_s

only through C_x (eq. 11). The entire behaviour of a fluid-filled crack oscillation is therefore described by C_x, α/a and χ, and does not depend separately on L_x/d and ρ_f/ρ_s. Although an analytical expression for the Q factors has yet to be obtained, this discovery may be a clue in future efforts to identify an expression for Q.

8 DISCUSSION AND CONCLUSIONS

The value of ϵ_m was found to be $\hat{g}_m$, that is, the average of the function g_m. Based on this discovery, we may explain the inverse proportionality between m and ϵ_m (eq. 44) as follows. Let $\langle|u_m|\rangle$ and $\langle|P_m|\rangle$ be average amplitude scales of u_m and P_m, respectively, and $\sigma_{zz}^{(s)}$ be the normal stress on the crack wall. The continuity of the normal stress across the crack wall suggests $\langle|P_m|\rangle \approx \langle|\sigma_{zz}^{(s)}|\rangle$, and the stress-strain relationship suggests $\langle|\sigma_{zz}^{(s)}|\rangle \approx \mu\langle|u_m|\rangle/\lambda_m$. Using these relationships and eq. (13), we obtain

$$\hat{g}_m \approx (\mu/L_x)(\langle|u_m|\rangle/\langle|P_m|\rangle) \approx \lambda_m/L_x \propto 1/m.\quad (56)$$

The inverse proportionality between m and ϵ_m is therefore explained in terms of the continuity of the normal stress and the stress–strain relationship.

We used eqs (23) and (31) to characterize the shape of the function g_m and obtained a best-fit γ value of 0.22 (Fig. 5). Fig. 8 shows the spatial distributions of u_m and P_m computed numerically, and Fig. 9 is a comparison of the numerical g_m values obtained by using the u_m/P_m ratios and analytical expressions for g_m based on eqs (23) and (31). In the analytical expressions, there is a flat region of g_m surrounded by a region of decreasing g_m amplitude toward the crack edges. The width of the flat region increases for larger χ and m, and that of the surrounding region decreases for larger m independent of χ. The transition from the flat to the surrounding region occurred at a distance $\gamma\lambda_m$ from each crack edge, and for the optimal value of $\gamma = 0.22$, the location of this transition was between the local maximum and node of u_m nearest to the crack edge (Fig. 8c); note that the waveforms were not sinusoidal because of the location-dependent wave speed (eq. 17), and thus the distance from the crack edge to the local maximum was not $\lambda_m/4$. The g_m values along y were in good agreement with eq. (31) (Figs 9a and b), whereas those along x showed discrepancies from the equation (Fig. 9c). This discrepancy was caused by the fact that g_m was defined as the u_m/P_m ratio that was unstable near the node locations of P_m. In particular, the node locations of u_m and P_m nearest to each crack edge differed slightly from each other (Fig. 8c). Consequently, there were large fluctuations of the numerically investigated g_m values (Fig. 9c). Despite these discrepancies, eqs (23) and (31) well predicted the resonance frequencies (Fig. 2; Maeda & Kumagai (2013)). Because the resonance frequencies were determined from an average of $[1 + 2C_x\bar{g}_m(x)]^{1/2}$ in our formulation (eqs 20 and 21), positive and negative discrepancies may have been cancelled out in this average. For example, the averages of $[1 + 2C_x\bar{g}_m(x)]^{1/2}$ for $m = 3$ (Fig. 9c) calculated with the equations and FDM solutions were 1.71 and 1.81, respectively, showing a difference of less than 10 per cent.

The fluid-filled crack model is one of the most widely used explanations for LP events at volcanoes. We previously proposed an empirical analytical expression for the resonance frequencies of the model (eqs 9 and 10) (Maeda & Kumagai 2013), but the applicability of the expression was limited because the values of ϵ_m^L and ϵ_m^W in these equations were given for only a few numbers of crack aspect ratios (W/L) and mode numbers (m). In the present study, we identified more broadly applicable expressions for the resonance
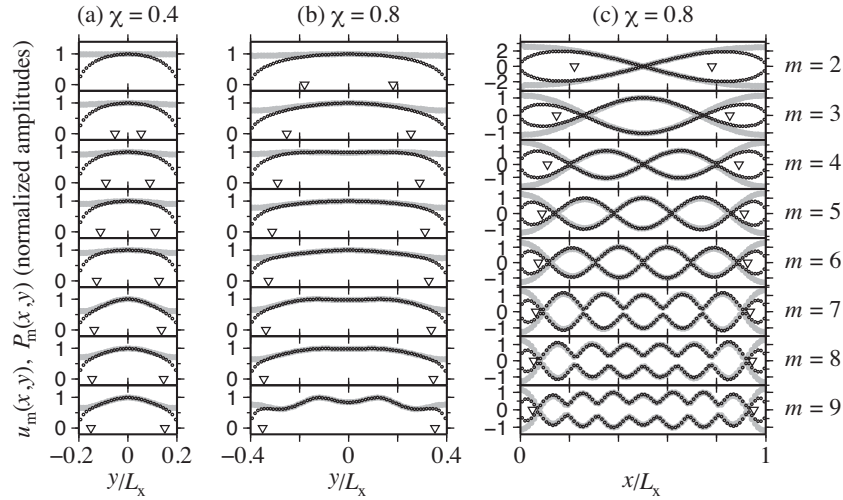
Figure 8. (a, b) A comparison of u_m (black circles) and P_m (grey circles) computed with the FDM for various values of χ and m along y at $x = 15L_x/32$ normalized by their maximum amplitudes and (c) along x at $y = 0$ normalized by their maximum amplitudes within $3L_x/8 \leq x \leq 5L_x/8$. We used $L_x/d = 10\,000$, $\rho_f/\rho_s = 1/120$ and $\alpha/a = 5$. Triangles indicate the locations that are by $\gamma\lambda_m$ apart from the nearest crack edge.
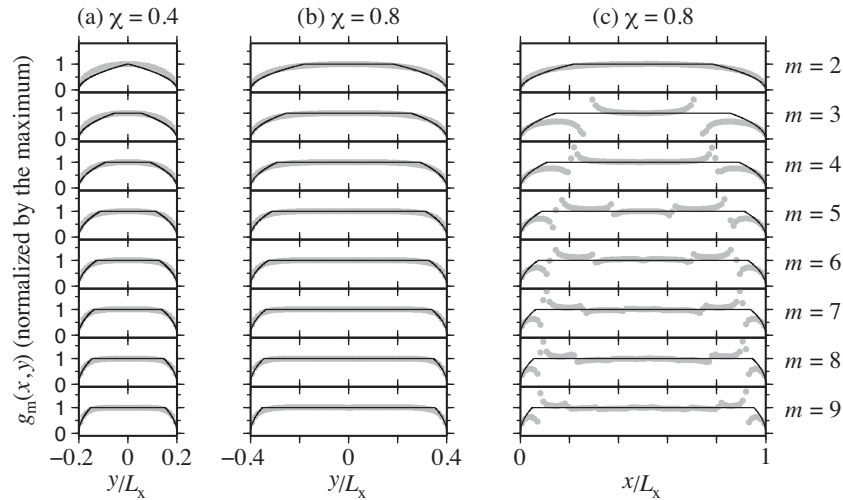

Figure 9. A comparison of g_m values computed with the FDM (grey circles) and eq. (31) (black lines) for various values of χ and m. The g_m values in panels (a) and (b) are along y at $x = 15L_x/32$, and those in panel (c) are along x at $y = 0$. We used $L_x/d = 10\,000$, $\rho_f/\rho_s = 1/120$ and $\alpha/a = 5$ in the FDM.

frequencies (eqs 47–52) that can be used for arbitrary W/L and m. Using these expressions, the resonance frequencies of cracks can be very easily predicted and can be compared to observed peak frequencies of LP events at volcanoes. Such comparisons may enhance our quantitative understanding of the processes that generate LP events.

The present study can be summarized as follows. We investigated theoretical expressions for the resonance frequencies of arbitrary rectangular fluid-filled cracks. To carry out this study, we assumed that the u_m/P_m ratio near each crack edge varied as the square root of the distance from the edge (eq. 23). Based on this assumption, we derived eqs (47)–(49) for a longitudinal mode and eqs (50)–(52) for a transverse mode. The predictions of these equations were in good agreement with numerical solutions (error in $f_m \leq 5$ per cent; Fig. 4a and eq. 40) for a wide range of crack aspect ratios. We showed that these equations can be well approximated (error ≤ 2 per cent; Fig. 2) by the empirical versions of eqs (9) and (10) that were proposed by Maeda & Kumagai (2013).

REFERENCES

Arciniega-Ceballos, A., Dawson, P. & Chouet, B.A., 2012. Long period seismic source characterization at Popocatepetl volcano, Mexico, *Geophys. Res. Lett.,* **39**(20), L20307, doi:10.1029/2012GL053494.

Bean, C.J., De Barros, L., Lokmer, I., Metaxian, J.-P., O'Brien, G. & Murphy, S., 2014. Long-period seismicity in the shallow volcanic edifice formed from slow-rupture earthquakes, *Nat. Geosci.,* **7,** 71–75.

Chouet, B., 1985. Excitation of a buried magmatic pipe: a seismic source model for volcanic tremor, *J. geophys. Res.,* **90**(B2), 1881–1893.

Chouet, B., 1986. Dynamics of a fluid-driven crack in three dimensions by the finite difference method, *J. geophys. Res.*, **91**(B14), 13 967–13 992.

Chouet, B.A. & Matoza, R.S., 2013. A multi-decadal view of seismic methods for detecting precursors of magma movement and eruption, *J. Volcanol. Geotherm. Res.*, **252**, 108–175.

Ferrazzini, V. & Aki, K., 1987. Slow waves trapped in a fluid-filled infinite crack: implication for volcanic tremor, *J. geophys. Res.*, **92**(B9), 9215–9223.

Gil Cruz, F. & Chouet, B.A., 1997. Long-period events, the most characteristic seismicity accompanying the emplacement and extrusion of a lava dome in Galeras Volcano, Colombia, *J. Volcanol. Geotherm. Res.*, **77**(1–4), 121–158.

Jousset, P. *et al.*, 2013. Signs of magma ascent in LP and VLP seismic events and link to degassing: an example from the 2010 explosive eruption at Merapi volcano, Indonesia, *J. Volcanol. Geotherm. Res.*, **261**, 171–192.

Julian, B.R., 1994. Volcanic tremor: Nonlinear excitation by fluid flow, *J. geophys. Res.*, **99**(B6), 11 859–11 877.

Kubotera, A., 1974. Volcanic tremors at Aso volcano, in *Physical Volcanology*, pp. 29–48, eds Civetta, L. *et al.*, Elsevier.

Kumagai, H., 2006. Temporal evolution of a magmatic dike system inferred from the complex frequencies of very long period seismic signals, *J. geophys. Res.*, **111**(B6), B06201, doi:10.1029/2005JB003881.

Kumagai, H., 2009. Source quantification of volcano seismic signals, in *Encyclopedia of Complexity and Systems Science,* pp. 9899–9932, ed. Meyers, R.A., Springer.

Kumagai, H. & Chouet, B.A., 2000. Acoustic properties of a crack containing magmatic or hydrothermal fluids, *J. geophys. Res.*, **105**(B11), 25 493–25 512.

Kumagai, H., Chouet, B.A. & Nakano, M., 2002. Temporal evolution of a hydrothermal system in Kusatsu-Shirane Volcano, Japan, inferred from the complex frequencies of long-period events, *J. geophys. Res.*, **107**(B10), 2236, doi:10.1029/2001JB000653.

Kumazawa, M., Imanishi, Y., Fukao, Y., Furumoto, M. & Yamamoto, A., 1990. A theory of spectral analysis based on the characteristic property of a linear dynamic system, *Geophys. J. Int.*, **101**(3), 613–630.

Maeda, Y. & Kumagai, H., 2013. An analytical formula for the longitudinal resonance frequencies of a fluid-filled crack, *Geophys. Res. Lett.*, **40**(19), 5108–5112.

Maeda, Y., Kumagai, H., Lacson Jr., R., Figueroa, M.S. II, & Yamashina, T., 2013. Source process of long-period seismic events at Taal volcano, Philippines: vapor transportation and condensation in a shallow hydrothermal fissure, *J. geophys. Res.*, **118**(6), 2832–2846.

Sun, C.T. & Jin, Z.-H., 2012. The elastic stress field around a crack tip, in *Fracture Mechanics,* pp. 25–75, Academic Press, Boston, doi:10.1016/B978-0-12-385001-0.00003-1.

Syahbana, D.K., Caudron, C., Jousset, P., Lecocq, T., Camelbeeck, T., Bernard, A. & Surono, 2014. Fluid dynamics inside a "wet" volcano inferred from the complex frequencies of long-period (LP) events: an example from Papandayan volcano, West Java, Indonesia, during the 2011 seismic unrest, *J. Volcanol. Geotherm. Res.*, **280**, 76–89.

Yamamoto, M. & Kawakatsu, H., 2008. An efficient method to compute the dynamic response of a fluid-filled crack, *Geophys. J. Int.*, **174**(3), 1174–1186.

APPENDIX A: ESTIMATING QUALITY (Q) FACTORS BASED ON THE FDM

The Q factors of a given waveform are usually estimated by the Sompi method (Kumazawa *et al.* 1990). However, the Sompi analysis yields several candidate Q values with some scatter. The analytical expression we needed requires a single Q value for each oscillation mode. We therefore estimated the Q factors using an alternative approach. We computed a far-field displacement waveform radiated by a resonating fluid-filled crack using the FDM code of Chouet (1986). We applied a cosine taper to the first and last $20L_x/\alpha$ time periods of the waveform and then band-pass filtered

between $0.9f_m$ and $1.1f_m$ (20 poles) to extract a damped oscillation for each mode m. We calculated local maxima of the band-passed waveform in a time interval $[t_b + 5/f_m, t_e - 10/f_m]$, where t_b and t_e define the time interval without tapering; however, if the global maximum appears after t_b, we replaced t_b with the time of the global maximum. We used this window of time to avoid the effects of an excitation of the resonance, the small amplitude portion at the end, and the tapers on both sides. We fitted the local maxima with an exponential function $A\exp(-\pi f_m t/Q_o)$, where A and Q_o are fitting parameters. We conducted this fitting using a log scale for the vertical axis.

The Q_o value represents the Q factor of the waveform that is affected by a numerical damping in the FDM. On the one hand, we used zero damping in the elastic medium because the absence of damping did not result in a numerical instability. On the other hand, we could not use zero damping in the fluid domain. We therefore needed to evaluate how numerical damping affected the estimated Q_o value. Numerical damping was expressed by a term $\rho_f c \nabla^2 v$ added on the right-hand side of the equation of motion in the fluid domain, where v is a fluid velocity. The constant c represents the strength of the numerical damping. Adding this term modified eq. (15) as follows:

$$\partial^2 P_m(x,t)/\partial t^2 = a_m(x)^2 \partial^2 P_m(x,t)/\partial x^2 + ca_m(x)^2 \partial^3$$
$$\times [P_m(x,t)/a_m(x)^2]/\partial t \partial x^2. \tag{A1}$$

Because $a_m(x)$ is a function of location x, the exact solution of this equation is difficult to derive. For a simple and approximate evaluation of the numerical damping effect, we approximated $a_m(x)$ by a constant a_m. Then eq. (A1) reduced to

$$\partial^2 P_m(x,t)/\partial t^2 = a_m^2 \partial^2 P_m(x,t)/\partial x^2 + c\partial^3 P_m(x,t)/\partial t \partial x^2. \tag{A2}$$

We considered a plane wave solution $P_m(x,t) = \exp[i(k_m x - \omega_m t)]$, where ω_m is an angular frequency and k_m is a wavenumber. Inserting this solution into eq. (A2) resulted in

$$k_m^2 = \omega_m^2 / (a_m^2 - i\omega_m c) = \omega_m^2 (a_m^2 + i\omega_m c) / (a_m^4 + \omega_m^2 c^2). \tag{A3}$$

The real and imaginary parts of eq. (A3) are

$$k_{mr}^2 - k_{mi}^2 = \omega_m^2 a_m^2 / (a_m^4 + \omega_m^2 c^2) \tag{A4}$$

and

$$2k_{mr}k_{mi} = \omega_m^3 c / (a_m^4 + \omega_m^2 c^2), \tag{A5}$$

respectively, where k_{mr} and k_{mi} are the real and imaginary parts of k_m. Dividing eq. (A4) by eq. (A5) gives $k_{mr}/k_{mi} - k_{mi}/k_{mr} = 2a_m^2/\omega_m c$. This equation has two solutions for k_{mr}/k_{mi}, and because k_{mr}/k_{mi} must be positive for a damped oscillation, we obtained

$$Q_n = k_{mr}/2k_{mi} = (1/2)\left\{ (a_m^2/\omega_m c) + \left[(a_m^2/\omega_m c)^2 + 1 \right]^{1/2} \right\}, \tag{A6}$$

where Q_n is an apparent Q factor caused by the numerical damping. The Q_o value includes this artifact but can be corrected as follows:

$$Q_c^{-1} = Q_o^{-1} - Q_n^{-1}, \tag{A7}$$

where Q_c represents the corrected Q factor.

We evaluated this correction method by repeating the Q_c estimations for the same crack with different numerical damping strengths c. We used a 2-D crack with $L_x/d = 10\,000$, $\rho_f/\rho_s = 1/120$, $\alpha/a = 5$, and we varied the non-dimensional damping strength $c' = c(\alpha/a)^2/\alpha\Delta x$ (Kumagai 2006), where Δx is the grid interval of the FDM computation ($\Delta x = L_x/80$ in our case). We varied
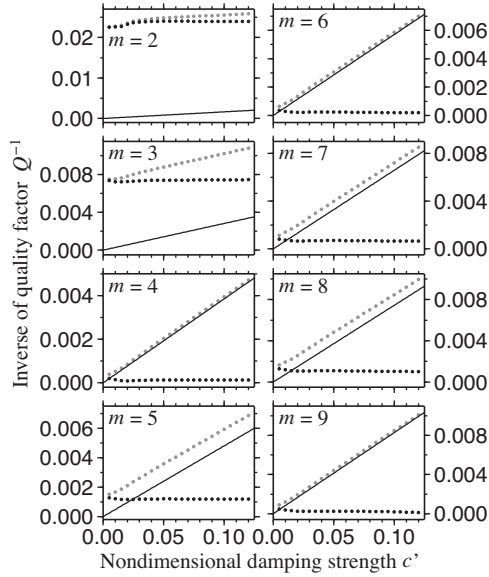
Figure A1. The quality (Q) factors estimated with the FDM using various values of non-dimensional damping strengths c'. Black lines represent the numerical damping effect (Q_n^{-1}) calculated with eq. (A6), and grey and black dots are Q_o^{-1} (without the numerical damping correction) and Q_c^{-1} (with the correction), respectively.

c' from 0.005 to 0.12 in increments of 0.005. On the one hand, the Q_o^{-1} values increased with c' (Fig. A1), indicating that Q_o was affected by the numerical damping. On the other hand, the Q_c^{-1} values calculated with eqs (A6) and (A7) were almost flat over a wide range of c' values (Fig. A1), suggesting that the numerical damping effect was successfully removed. Based on this evaluation, we adopted Q_c (for $c' = 0.075$) as our final estimation of the Q factor.

When Q_o and Q_n are very close to each other, a small error in either of them results in a large error in Q_c (eq. A7). To avoid this
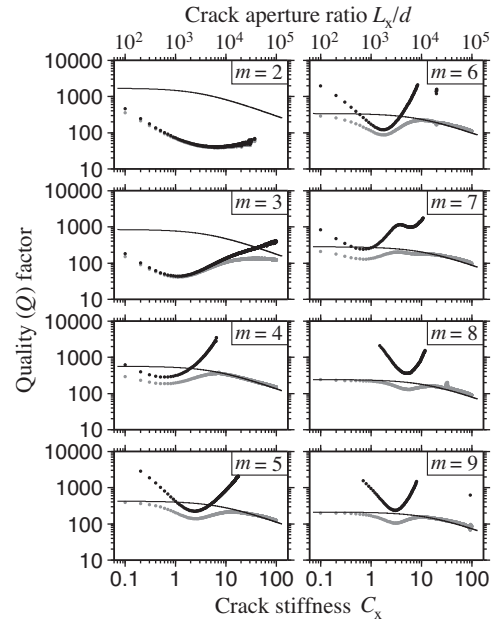

Figure A2. The quality factors of 2-D cracks without (Q_o; grey) and with (Q_c; black) corrections for numerical damping. The results corresponding to Fig. 7 with varying L_x/d and fixed values of ρ_f/ρ_s and α/a are shown. Black lines represent Q_n values calculated with eq. (A6).

problem, we used a threshold $Q_o < 0.9Q_n$ for our calculation of Q_c. In Fig. A2, we compare the Q_o, Q_n, and Q_c values for various crack stiffnesses. The number of data points for Q_c is smaller than for Q_o because of the threshold. For $C_x > 10$ in particular, we could not estimate Q_c in most cases because of significant numerical damping effects. The Q_c values were relatively well determined for the range $1 < C_x < 10$ (Fig. A2).